Analyst

PAPER

View Article Online
View Journal

Cite this: DOI: 10.1039/d5an01241d

Selective detection of lipophagy with a highly specific lipid droplet probe

Shixiong Wen,†[a] Xiaoxue Zou,†[b] Jianing Liu,[b] Jiahuai Han*[a,c] and Shoufa Han *[a,b]

Received 26th November 2025,
Accepted 23rd March 2026

DOI: 10.1039/d5an01241d

rsc.li/analyst

Lipophagy, the autophagic degradation of lipid droplets (LDs) by lysosomes, is an important route for maintaining LD homeostasis. Tools for lipophagy detection facilitate research in LD biology. Herein, we report LD-Blue, a highly specific LD probe, for tracking dynamic formation of LDs and detection of lipophagy. Upon lipophagy, LD-Blue chaperoning host LDs is delivered into lysosomes. By using the co-localization co-efficiency of LD-Blue and LysoTracker Red as the readout of lipophagy, we observed lipophagy induced by serum deprivation but not acute nutrient starvation as well as lipophagy inhibition by chloroquine and Bafilomycin A1. With the established fidelity of the LD-Blue-based co-localization assay for lipophagy, monensin is identified to be a potent inducer of lipophagy.

Lipid droplets (LDs), vesicular organelles enclosed by a single phospholipid layer, are the central hub coordinating cellular lipid uptake, storage, distribution and utilization. Predominantly found in adipocytes and hepatocytes,[1] the catabolism of LDs occurs primarily through two pathways: lipolysis and lipophagy.[2] The latter, a selective autophagy process, involves engulfment of LDs by autophagosomes that are further fused with lysosomes for degradation.[3] As dysregulated lipophagy is associated with a spectrum of pathologies including obesity, diabetes and hepatic disorders,[4] tools allowing accurate detection of lipophagy are beneficial for investigating lipophagy-engaged diseases. In this regard, stringent probe specificity for LDs is a prerequisite for tracking dynamics of LDs and lipophagy. Much effort has been directed to the development of LD probes with improved performance,[5,6] often by integrating lipophilic fluorophores such as BODIPY,[7] coumarin,[8] triphenylamine[9] and 1,8-naphthalimide.[10] In addition, LD probes have been used to differentiate cancerous cells from normal cells.[11] Lipophagy has been assessed by electron microscopy, immunofluorescence staining or co-localization co-efficiency of fluorescent protein-defined lysosomes with dye-stained LDs.[3,12] Chemical imaging probes are more advantageous than protein-based ones in several aspects, such as applicability to diverse cell lines and ease of structural modification. Currently, there remains a paucity of chemical probes suitable for lipophagy imaging.[8d,13] Based on the advances of LD dyes, we herein disclose LD-Blue, a highly specific probe for imaging dynamic LDs and lipophagy. LD-Blue consists of a hydrophobic fluorogen of 1,8-naphthalimide and an entity of 3,5-bis(trifluoromethyl) benzene. Weakly fluorescent under polar conditions, LD-Blue becomes highly emissive in hydrophobic LDs. Upon lipophagy, LDs are delivered into lysosomes, leading to varied overlap co-efficiency of LD-Blue trapped in LDs with LysoTrackers in lysosomes. Utilizing this overlap/co-localization assay, we observed that robust lipophagy was induced by serum deprivation but not acute nutritional deficiency, such as Hanks buffered salt solution (HBSS) treatment. The latter is often employed to trigger autophagy of organelles including mitochondria and endoplasmic reticulum. With LD-Blue, monensin is found to be a potent inducer of lipophagy (Scheme 1).

Experimental procedure

Materials and methods

Cell lines and reagents. HeLa (CCL-2™), SH-SY5Y (CRL-2266™), Hep G2 (HB-8065™), A549 (CCL-185), and MCF-7 (HTB-22™) cells were obtained from the American Type Culture Collection (ATCC). MEF cells were a gift from the laboratory of Professor Chen-Song Zhang. HeLa cells stably expressing LAMP2-GFP (Lyso-GFP), TOMM20-RFP (Mito-RFP), SS-RFP (ER-RFP), and TMEM165-RFP (GA-RFP) were kindly provided by Professor Jiahuai Han's laboratory. All cell lines were cultured with Dulbecco's modified Eagle's medium (DMEM; GIBCO, C11995500CP) supplemented with 10% fetal bovine serum (Thermo, A3160901), 2 mM L-glutamine, 100 IU

[a]Academician Workstation of Immune Cell Signal Transduction, School of Basic Medicine, Chongqing Medical University, Chongqing, 400016, China. E-mail: shoufa@xmu.edu.cn, jhan@xmu.edu.cn
[b]Department of Chemical Biology, College of Chemistry and Chemical Engineering, State Key Laboratory for Physical Chemistry of Solid Surfaces, the Key Laboratory for Chemical Biology of Fujian Province, the MOE Key Laboratory of Spectrochemical Analysis & Instrumentation, Xiamen University, Xiamen 361005, China
[c]State Key Laboratory of Cellular Stress Biology, Innovation Center for Cell Signaling Network, School of Life Sciences, Xiamen University, Xiamen 361005, China
† Both of these authors contributed equally to this work.

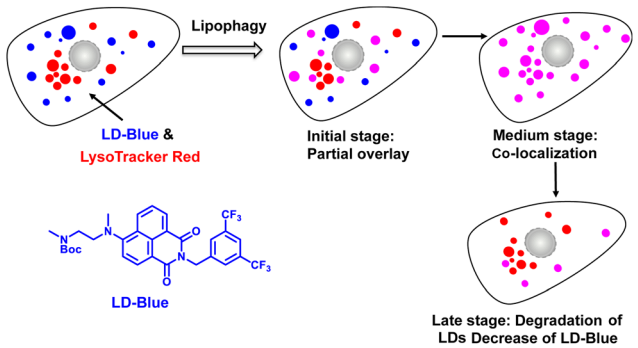

Scheme 1 Schematic for lipophagy detection with LD-Blue. Lipophagy leads to delivery of LD-Blue-trapped LDs into lysosomes. Thus, the level of overlap/co-localization of fluorescence signals of LD-Blue and LysoTracker Red serves as the index of lipophagy. Attenuation of LD-Blue signals following co-localization due to degradation of LDs serves as another corroborative readout for lipophagy.

penicillin, and 100 mg mL^{-1} streptomycin at 37 °C in a humidified incubator under 5% CO_2. Tunicamycin (HY-A0098), thapsigargin (HY-13433), rapamycin (HY-10219), etoposide (HY-13629), carbonyl cyanide *m*-chlorophenylhydrazone (CCCP, HY-100941), rotenone (HY-B1756), nigericin (HY-127019), monensin (HY-N0150), chloroquine (CQ, HY-17589A), BODIPY 493/503 (HY-W090090), LysoTracker Red (HY-D1300) and Nile Red (HY-D0718) were purchased from MCE. Hoechst (C1017), Golgi-Tracker Red (C1043), oleic acid (OA, ST2053), HBSS (Hanks' Balanced Salt Solution with Ca^{2+} & Mg^{2+}, C0219), Cell Counting Kit-8 (C0037) and ER-Tracker Red (C1041S) were purchased from Beyotime. MitoTracker Deep Red (MTDR, M22426) was purchased from Invitrogen. Bafilomycin A1 (Baf-A1; S1413) was purchased from Selleck. All other chemicals were purchased from Sigma unless specified.

Microscopy. The fluorescence spectra were recorded on a SpectraMax M5 (Molecular Devices). Confocal fluorescence microscopy imaging was performed on a Zeiss LSM 980 using the following filters: λ_{ex} = 488 nm/λ_{em} = 499–553 nm for BODIPY 493/503 and GFP; λ_{ex} = 561 nm/λ_{em} = 570–620 nm for RFP, Nile Red, ER-Tracker Red and LysoTracker Red; λ_{ex} = 633 nm/λ_{em} = 645–700 nm for MitoTracker Deep Red; λ_{ex} = 405 nm/λ_{em} = 410–440 nm for Hoechst; and λ_{ex} = 445 nm/λ_{em} = 490–560 nm for LD-Blue. Images of merged fluorescence were processed using ZEN 3.4 (blue edition). Graphs were generated using GraphPad Prism 8 and Origin 2019 software. All cells analysed by confocal microscopy were seeded in 35 mm glass-bottom cell culture dishes.

Synthesis of LD-Blue

To a flask containing 4-bromo-1,8-naphthalic anhydride (2.8 g) in DMF (50 mL) were added 3,5-bis(trifluoromethyl)benzylamine (2.4 g) and sodium carbonate (2 g). The mixture was stirred at 50 °C for 4 h and then charged with *N*,*N*′-dimethyl ethylenediamine (4.0 g). The mixture was further stirred at 70 °C for 8 h, concentrated and then extracted with EtOAc (200 mL) against aqueous hydrochloride solution (1 M, 200 mL). The organic layer was collected, desiccated with sodium sulfate and then concentrated. The residue was dissolved in dichloromethane (50 mL). To the solution was added TEA (10 mL) and di-*tert*-butyl bicarbonate (6 g). The solution was stirred at room temperature for 2 h and then concentrated under reduced pressure. The residue was purified by silica gel column chromatography using petroleum ether/ethyl acetate (PE/EA, 3 : 1 to 1 : 1) as the eluent to give LD-Blue in 49% yield (3.0 g). ^{1}H NMR (500 MHz, $CDCl_3$) δ (ppm) 8.57 (d, J = 7.23 Hz, 1H), 8.47 (dd, J = 18.07, 8.2 Hz, 2H), 8.00 (s, 1H), 7.75 (s, 1H), 7.66 (d, J = 7.88 Hz, 1H), 7.45 (t, J = 7.45 Hz, 1H), 7.17–7.09 (m, 1H), 5.43 (s, 2H), 3.55 (d, J = 17.7 Hz, 3H), 3.13 (d, J = 14.6 Hz, 3H), 2.65 (s, 1H), 2.33 (s, 1H), 1.46–1.35 (s, 9H). ^{13}C NMR (126 MHz, $CDCl_3$) δ (ppm) 164.46, 163.81, 140.10, 133.04, 132.03, 131.77, 131.62, 131.50, 131.24, 131.09, 130.32, 129.30, 129.00, 128.19, 126.55, 126.06, 125.72, 125.46, 125.27, 125.18, 124.38, 122.65, 122.21, 121.51, 121.48, 121.45, 121.42, 121.39, 115.30, 115.03, 114.86, 114.67, 79.74, 54.69, 54.14, 46.44, 46.17, 42.65, 42.23, 34.73, 34.58, 28.36. ^{19}F NMR (565 MHz, $CDCl_3$) δ (ppm) −62.70. MS (ESI): $C_{30}H_{29}F_6N_3O_4Na^+$ calculated: 632.549; found: 632.401.

Selectivity of LD-Blue for LDs

MEF cells were cultured in DMEM containing LD-Blue (2 μM, 1 h), referred to as LD-Blue$^+$ cells. The cells were washed and then incubated with Nile Red (2 μM, 1 h) or BODIPY 493/503 (2 μM, 1 h). The cells were washed three times with phosphate-buffered saline (PBS), maintained in fresh DMEM and then imaged by confocal microscopy.

MEF cells, Hep G2 cells, SH-SY5Y cells, HeLa cells, A549 cells, and MCF-7 cells were cultured for 1 h in DMEM containing LD-Blue (2 μM) and BODIPY 493/503 (2 μM). The resultant cells were washed three times with PBS, maintained in DMEM and imaged by confocal microscopy.

LD-Blue$^+$ MEF cells were incubated with Hoechst (0.5 μg mL^{-1}, 0.5 h), LysoTracker Red (1 μM, 1 h), MitoTracker Deep Red (0.15 μM, 15 min), ER-Tracker Red (1 μM, 1 h) and Golgi-Tracker Red (1 μM, 1 h), respectively. The cells were washed three times with PBS, maintained in DMEM, and then imaged by confocal microscopy.

HeLa cells expressing LAMP2-GFP (Lyso-GFP), TOMM20-RFP (Mito-RFP), SS-RFP (ER-RFP), and TMEM165-RFP (GA-RFP) were stained with LD-Blue (2 μM, 1 h), washed three times with PBS, maintained in DMEM and then imaged by confocal microscopy.

Tracking oleic acid-promoted LD biosynthesis with LD-Blue

MEF cells, SH-SY5Y cells, HeLa cells, and MCF-7 cells were independently cultured in DMEM supplemented with oleic acid (200 μM, 12 h). These cells were further cultured with LD-Blue (2 μM, 1 h) or BODIPY 493/503 (2 μM, 1 h). The cells were washed three times with PBS, maintained in fresh DMEM, and then imaged by confocal microscopy.

Photostability of LD-Blue

LD-Blue was dissolved in PBS (10 mM, pH 7.5) containing dimethyl sulfoxide (DMSO, 30%, v/v) to a final concentration of

2 μM. The solution was continuously irradiated under λ_{ex} = 410 nm for 1 h, with fluorescence intensity recorded at 10 min intervals.

LD-Blue$^+$ MEF cells were subjected to confocal microscopy under continuous 450 nm excitation for 1 h. *Z*-Stack images were acquired at 10 min intervals (0–60 min) for fluorescence decay analysis.

Cytotoxicity of LD-Blue

MEF cells were incubated with LD-Blue (0 μM, 1 μM, 2 μM, 5 μM, 10 μM) for varied periods of time (0 h, 24 h, or 48 h). The cells were washed three times with PBS, and then maintained in fresh DMEM. Cell cytotoxicity was measured with a CCK-8 kit according to the manufacturer's guidelines.

Effects of cell fixation on staining LDs with LD-Blue

MEF cells pre-stained with LD-Blue or BODIPY 493/503 were fixed with 4% paraformaldehyde (PFA). In parallel, MEF cells were first fixed with 4% PFA and then stained with LD-Blue (2 μM, 1 h) or BODIPY 493/503 (2 μM, 1 h) in DMEM. All cell samples were subjected to confocal microscopy for fluorescence imaging analysis.

LD formation in HBSS-treated cells revealed by LD-Blue

MCF-7 cells were maintained in HBSS for 0 h (control) or 6 h, and then stained with LD-Blue (2 μM, 1 h). The cells were washed three times with PBS, maintained in DMEM and then immediately imaged by confocal laser microscopy.

Imaging lipophagy with LD-Blue

Starvation-induced lipophagy. MEF cells, HeLa cells and SH-SY5Y cells were cultured with LysoTracker Red (1 μM, 1 h) and LD-Blue (2 μM, 1 h). The cells, referred to as LysoTracker Red$^+$/LD-Blue$^+$ cells, were maintained for 24 h in serum-free DMEM, in HBSS, or in DMEM (control). The cells were analyzed by confocal microscopy.

Inhibition of lipophagy. LysoTracker Red$^+$/LD-Blue$^+$ MEF cells were cultured for 24 h in serum-free DMEM spiked with Bafilomycin A1 (Baf-A1, 25 nM), chloroquine (CQ, 10 μM) or with no addition. Cells were subsequently analyzed by confocal laser microscopy.

Effects of pharmocological agents on lipophagy. LysoTracker Red$^+$/LD-Blue$^+$ MEF cells were maintained for 24 h in DMEM containing the following compounds (10 μM): thapsigargin, tunicamycin, rotenone, CCCP, nigericin, monensin, etoposide, or rapamycin, respectively. Cells were washed three times with PBS, maintained in fresh DMEM and then imaged by confocal microscopy.

Time-course study of lipophagy induced by monensin. LD-Blue$^+$ MEF cells were maintained in serum-free DMEM or DMEM spiked with monensin (10 μM) for 1 h, 6 h, 12 h or 24 h. The cells were stained with LysoTracker Red (1 μM, 1 h) and then analyzed by confocal laser microscopy.

Decrease of LDs upon lipophagy

MEF cells were maintained in serum-free DMEM or DMEM spiked with monensin (10 μM) for 24 h and then stained with LD-Blue (2 μM, 1 h). Cells were analyzed by confocal laser microscopy for levels of LDs.

Results and discussion

Synthesis and characterization of LD-Blue

We first syntheszied LD-Blue *via* a three-step procedure (Fig. 1A). Titration showed that LD-Blue exhibited green fluorescence that increased dramatically in a nonpolar medium (dioxane) (Fig. 1B and C), suggesting its utility for fluorogenic staining of hydrophobic LDs.

Selectivity of LD-Blue for LDs

We first examined probe specificity for LDs by co-culturing MEF cells with LD-Blue and commercial probes for LDs (BODIPY 493/503 or Nile Red; Fig. 2A). We observed discrete punctate blue-fluorescent structures where these punctate dots are co-stained with BODIPY 493/503 or Nile Red (Fig. 2B). Both commercial probes exhibit obvious background fluorescence, whereas LD-Blue produced no detectable signals outside LDs (Fig. 2B and C), demonstrating the selectivity of LD-Blue for LDs. We further incubated LD-Blue with MEF, Hep G2, SH-SY5Y, HeLa, A549 and MCF-7 cells using BODIPY 493/503 as the control. Confocal microscopy analysis revealed that LD-Blue effectively labeled LDs in all tested cell lines with minimal nonspecific staining (Fig. 3A and B). In addition, we observed varied fluorescence intensity levels in a cell-type dependent manner (Fig. 3A), reflecting varied LD abundance in these cell lines.

To further verify the specificity of LD-Blue, we co-stained MEF cells with LD-Blue and different organelle markers including Hoechst (nucleus), LysoTracker Red (lysosomes), MitoTracker Deep Red (mitochondria), ER-Tracker Red (endoplasmic reticulum), and Golgi-Tracker Red (Golgi apparatus). Confocal microscopy analysis revealed no detectable overlap between LD-Blue and all the organelle markers examined

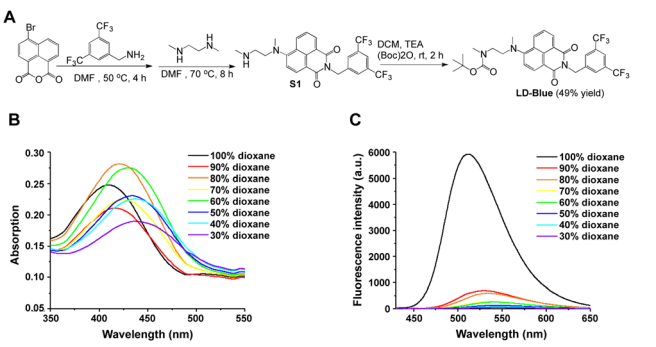

Fig. 1 Optical properties of LD-Blue. (A) Synthetic route for LD-Blue. Polarity-related fluorescence emission of LD-Blue. LD-Blue was added to phosphate buffered saline (PBS, 10 mM, pH 7.5) containing 30–100% dioxane to a final concentration of 10 μM. These aqueous samples were analysed for UV-vis absorbance (B) and fluorescence emission (C) using λ_{ex} = 410 nm.

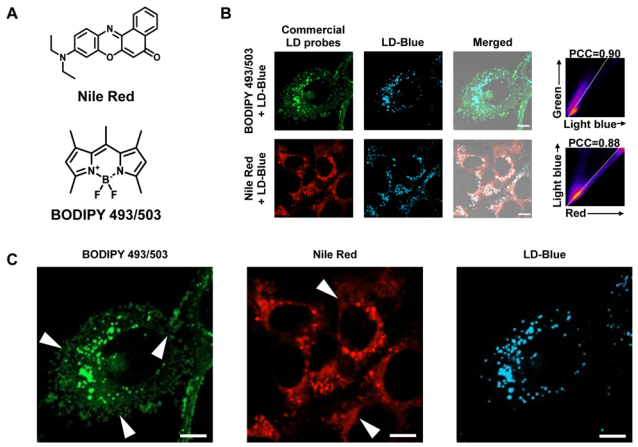

Fig. 2 Stringent selectivity of LD-Blue for LDs. (A) Chemical structure of BODIPY 493/503 and Nile Red. (B) Selectivity of LD-Blue for LDs as compared to commercial LD-probes. MEF cells were stained with LD-Blue (2 μM, 1 h) and then with Nile Red (2 μM, 1 h) or BODIPY 493/503 (2 μM, 1 h) at 37 °C. The cells were washed with PBS three times and then visualized by confocal microscopy. (C) Enlarged images of LDs stained with LD-Blue over commercial probes. The white arrows indicate non-specific signals of the commercial probes. Scale bars: 10 μm.

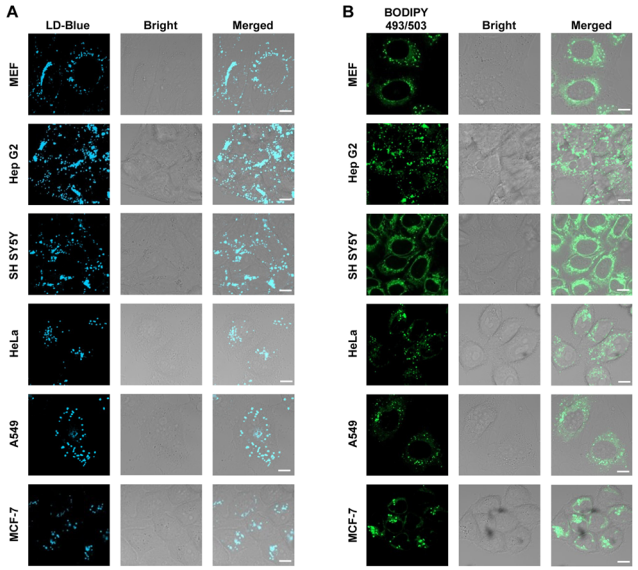

Fig. 3 Applicability of LD-Blue for LD staining in different cell lines. MEF, Hep G2, SH-SY5Y, HeLa, A549, and MCF-7 cells were stained with (A) LD-Blue (2 μM, 1 h) or (B) BODIPY 493/503 (2 μM, 1 h), respectively. The cells were washed three times with PBS, then maintained in fresh DMEM and imaged by confocal microscopy. Scale bars: 10 μm.

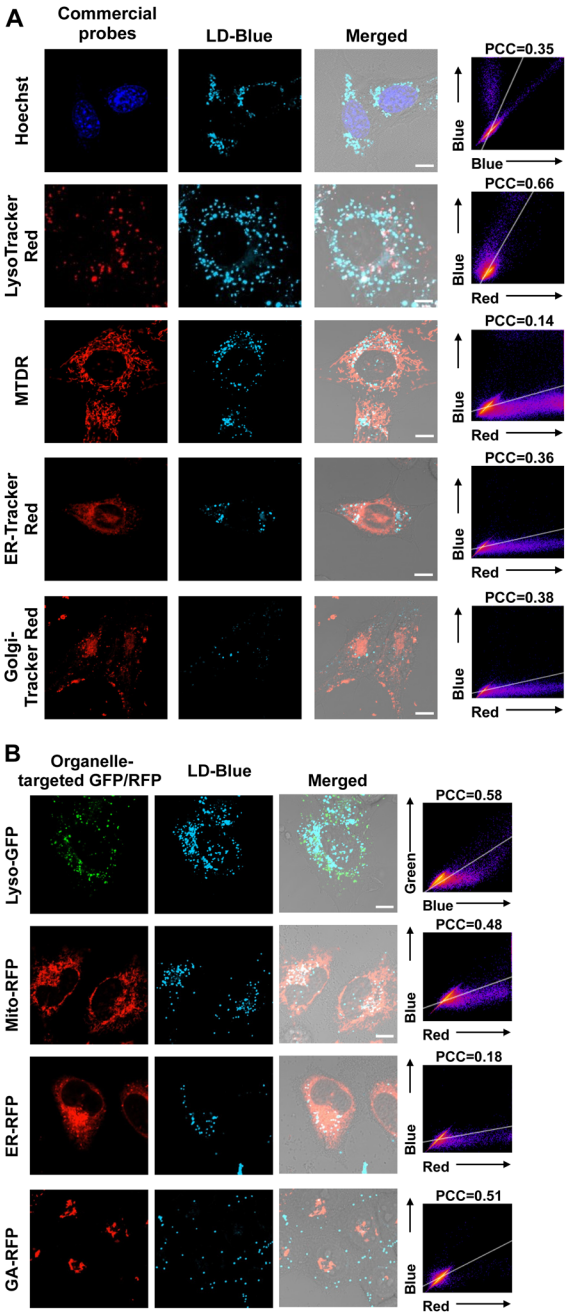

Fig. 4 Selectivity of LD-Blue for LDs over other organelles. (A) LD-Blue$^+$ MEF cells were stained with Hoechst (0.5 μg mL^{-1}, 0.5 h), LysoTracker Red (1 μM, 1 h), MitoTracker-Deep Red (MTDR, 0.15 μM, 15 min), ER-Tracker Red (1 μM, 1) or Golgi-Tracker Red (1 μM, 1 h). The cells were washed three times with PBS and then maintained in fresh DMEM prior to confocal microscopy analysis. (B) HeLa cells expressing different organelle-specific fluorescent proteins were stained with LD-Blue (2 μM, 1 h), washed three times with PBS, maintained in fresh DMEM and then imaged by confocal microscopy. Scale bars: 10 μm.

(Fig. 4A). This pattern was also observed in HeLa cells expressing fluorescent protein-tagged organelle markers: LAMP2-GFP for lysosomes (referred to as Lyso-GFP), TOMM20-RFP, specific for mitochondria (referred to as Mito-RFP), SS-RFP for endoplasmic reticulum (referred to as ER-RFP), and TMEM165-RFP for Golgi apparatus (GA-RFP) (Fig. 4B). Taken together, these results show stringent specificity of LD-Blue for LDs over other organelles and the applicability of LD-Blue to diverse cell lines.

Since LD-Blue is non-fluorescent in aqueous media but fluorogenic within LDs (Fig. 1–5), we next assessed LD-Blue for

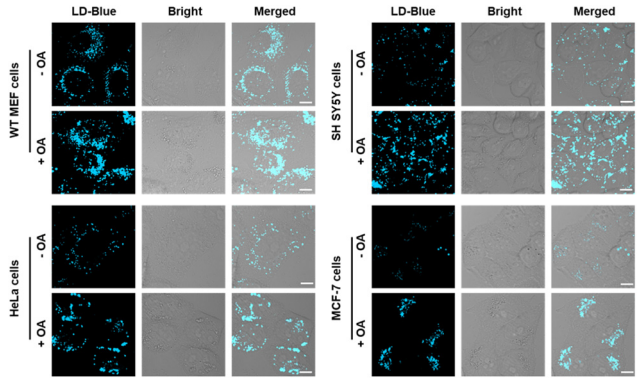

Fig. 5 Tracking LD biosynthesis in OA-treated cells by LD-Blue. MEF cells, SH-SY5Y cells, HeLa cells, and MCF-7 cells were cultured with OA (200 μM, 12 h) and then stained with LD-Blue (2 μM, 1 h). The cells were washed three times with PBS, maintained in fresh DMEM, and then imaged by confocal microscopy. Scale bar: 10 μm.

tracking dynamic changes of LD levels by treating MEF, SH-SY5Y, HeLa and MCF-7 cells with oleic acid (OA).[14] OA could activate the long-chain fatty acid receptor FFAR4, leading to significant increases in cellular LDs.[14a] Cell analysis revealed marked enhancement of LD-Blue-positive dots in OA-treated cell lines but not control cell lines free of OA treatment (Fig. 5A–D). OA-induced LD formation was also confirmed by BODIPY 493/503 (Fig. S1A–D, SI). Collectively, these findings demonstrate the capability of LD-Blue to detect dynamic changes of metabolism in LDs. The serendipitous discovery that LD-Blue is highly selective for LDs, unlike previously reported 1,8-naphthalimide-derived LD probes lacking a trifluoromethyl group, indicates that the $-CF_3$ substituent imparts a unique property that favors probe partitioning into hydrophobic LDs.

Imaging of lipophagy using LD-Blue

Prior to lipophagy analysis, LD-Blue was assessed for its biocompatibility. We identified negligible cytotoxicity in MEF cells treated with LD-Blue up to 10 μM for 48 h (SI, Fig. S2A). In addition, no significant decrease in fluorescence intensity was observed after continuous excitation of LD-Blue for 1 h either *in vitro* or in live cells (SI, Fig. S2B and C), showing excellent photostability. This is beneficial for real-time bioimaging. Lastly, LD-Blue could stain LDs in cells pre-fixed with paraformaldehyde; additionally, it is well retained in LDs after cell fixation (SI, Fig. S2D and E). These advantages of LD-Blue demonstrate that it is capable of staining LDs both in live cells and fixed cells.

Complete nutrient deprivation such as HBSS treatment promotes autophagy of mitochondria,[15] Golgi apparatus,[16] and endoplasmic reticulum.[17] However, it has been reported that acute nutrient stress (HBSS treatment) did not induce lipophagy, whereas milder conditions such as serum-free starvation significantly triggers lipophagy.[18] Surprisingly lipophagy induced by HBSS treatment has also been reported using synthetic chemical probe-based assays.[13a,b] Given this discrepancy, we applied LD Blue to the investigation of lipophagy under both starvation conditions.

LD-Blue$^+$/LysoTracker Red$^+$ cells were maintained in HBSS or serum-free DMEM. Confocal microscopy imaging showed that cells starved in serum-free DMEM exhibited massive LD-Blue signals that co-localized with LysoTracker Red with a Pearson's correlation coefficient (PCC) of 0.91 (Fig. 6B), showing delivery of LDs into lysosomes, a hallmark of lipophagy. Moreover, the level of co-localization increases in a time-dependent manner (SI, Fig. 7), consistent with accumulation of LDs within lysosomes in lipophagy. Meanwhile, the overall fluorescence level of LD-Blue in serum-starved MEF cells is significantly reduced (SI, Fig. S3), reflecting degradation of LDs, another hallmark of lipophagy. Importantly, no enhanced co-localization of LD-Blue with LysoTracker Red was identified in cells starved in HBSS (PCC = 0.30) relative to non-starved control cells (PCC = 0.37) (Fig. 6B), showing that HBSS is incapable of inducing lipophagy. This pattern was also observed in HeLa and SH-SY5Y cells (SI, Fig. S4), reinforcing that serum starvation rather than complete nutrient deprivation triggers lipophagy. Our findings are consistent with prior report on lipophagy induced by serum starvation, but not acute nutrient stress.[18] Moreover, we observed higher levels of LDs outside of lysosomes in HBSS-treated MCF-7 cells (SI, Fig. S5). As MCF-7 cells exhibit inherently low abundance of LDs, the enhanced populations of LDs that are observed indicate that acute nutrient starvation does not trigger lipophagic

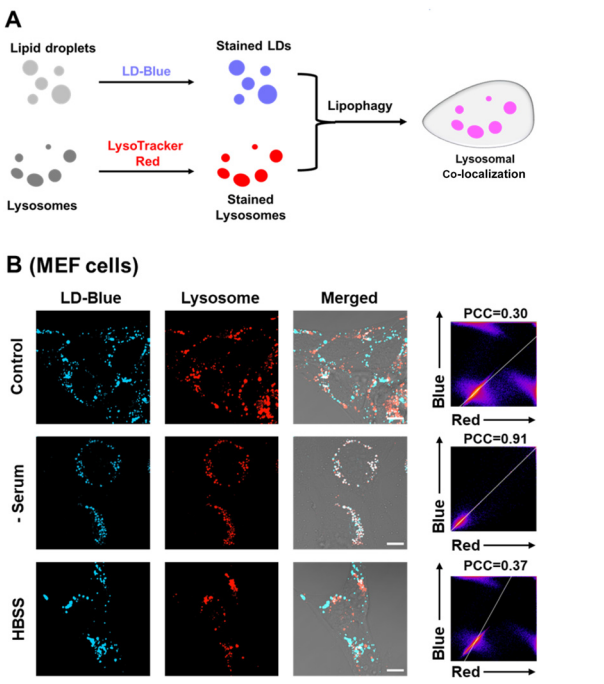

Fig. 6 Detection of lipophagy with LD-Blue. (A) Scheme of overlap coefficiency-based lipophagy detection with LD-Blue and LysoTracker Red. (B) Lipophagy induced by serum starvation and biosynthesis of LDs induced by starvation in HBSS. LD-Blue$^+$ MEF cells were subjected to either serum starvation or HBSS treatment, and then imaged by confocal microscopy. Scale bar: 10 μm.

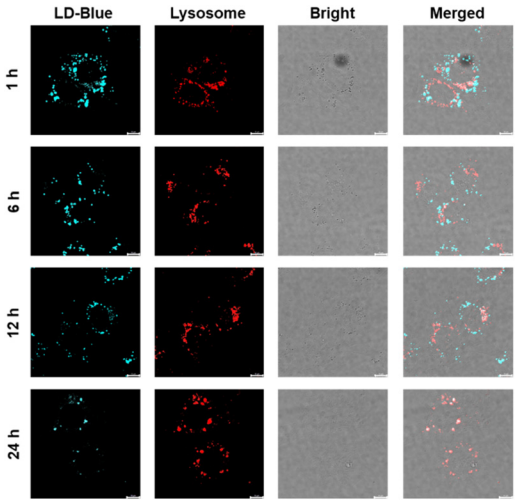

Fig. 7 Time-course study on the levels of LDs and lysosome–LD co-localization in serum-deprived MEF cells. LD-Blue$^+$ MEF cells were maintained in serum-deprived DMEM or complete DMEM for 1, 6, 12 and 24 h, respectively, and then stained with LysoTracker Red (1 μM, 1 h). Cells were analyzed by confocal laser microscopy.

flux but instead stimulates LD biogenesis. This is consistent with a prior report on HBSS-promoted LD biogenesis.[18]

During initiation of lipophagy, LD-specific protein PLIN2 is degraded *via* the chaperone-mediated autophagy (CMA) pathway.[12a] Consequently, the autophagic status of LDs can be assessed by monitoring changes in PLIN2 protein levels. We observed a marked reduction of PLIN2 in serum-deprived cells, whereas acute nutrient deprivation triggered a sharp increase in PLIN2 abundance (SI, Fig. S6), validating the occurrence of lipophagy in LD-Blue$^+$ cells subjected to mild starvation but not HBSS treatment.

To further prove the selectivity of the LD-Blue-based co-localization assay for lipophagy, we treated serum-starved cells with Baf-A1 that blocks autophagy by inhibiting fusion of lysosomes with autophagosomes but also inhibits V-ATPase to neutralize lysosomes.[19] Baf-A1 treatment caused dissipation of acidotropic LysoTracker due to loss of lysosomal acidity where LD-Blue signals were largely unaffected (SI, Fig. S7). As lipophagy leads to degradation of LDs, the retention of LD-Blue signals reflects lipophagy inhibition by Baf-A1. Chloroquine (CQ) inhibits autophagy by preventing binding of autophagosomes to lysosomes.[20] We observed massive LD-Blue signals from LDs outside lysosomes (SI, Fig. S7), in line with inhibited lipophagy by CQ. Together, these data validate the fidelity of the LD-Blue assay for lipophagy.

Identification of lipophagy inducers with LD-Blue

Mitophagy induces transformation of brown adipocytes into white adipocytes.[21] Mitochondrial oxidative phosphorylation promotes endoplasmic reticulum autophagy.[22] These studies inspired us to examine known organelle stressors for their capability to induce lipophagy. Therefore, LysoTracker Red$^+$/LD-Blue$^+$ MEF cells were treated with endoplasmic reticulum stressors (thapsigargin, tunicamycin), mitochondrial stressors (rotenone, CCCP), Golgi apparatus stressors (nigericin, monensin), and general autophagy inducers (etoposide, rapamycin) and then imaged by confocal microscopy. This revealed that monensin caused the most robust lipophagy (PCC = 0.87) that increased in a time-dependent manner (Fig. 8 and SI, Fig. S8). Consistent with the enhanced overlap co-efficient, the overall fluorescence of LD-Blue in serum-deprived MEF cells is significantly reduced (SI, Fig. S9), indicating degradation of LDs by lipophagy. Moreover, monensin-treated cells exhibited a significant decrease in PLIN2 levels (SI, Fig. S6), further confirming the occurrence of lipophagy. Overall, our results showed that monensin is an effective inducer of lipophagy.

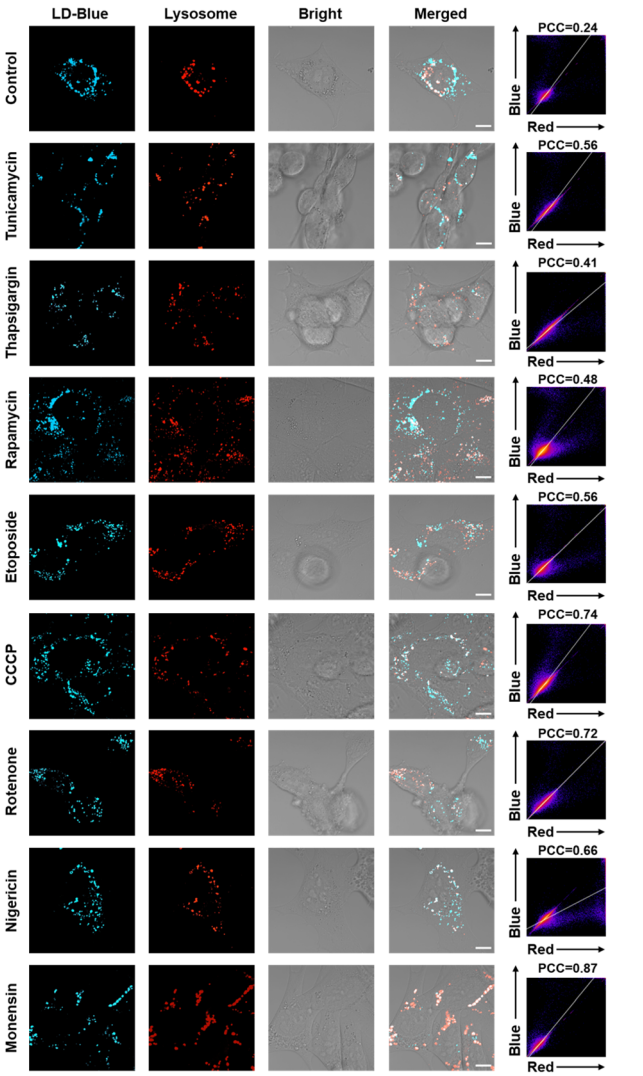

Fig. 8 Identification of monensin as a lipophagy inducer by LD-Blue. LysoTracker Red$^+$/LD-Blue$^+$ MEF cells were treated with each of the following compounds (10 μM, 24 h): thapsigargin, tunicamycin, rotenone, CCCP, nigericin, monensin, etoposide and rapamycin. Cells were washed three times with PBS prior to confocal microscopic analysis. Scale bar: 10 μm.

Conclusion

Given the causal role of lipophagy in several diseases and the current lack of specific imaging probes, we herein disclose LD-Blue as a suitable tool for the detection of dynamic LD levels and lipophagy by monitoring increased fluorescence overlap co-efficiency between LD-Blue and lysosomal markers, as well as the attenuation of LD-Blue signals resulting from LD degradation. The latter provides a corroborative indicator of lipophagy. The fidelity of the LD-Blue-based co-localization assay for lipophagy was validated by detecting lipophagy triggered by mild starvation, but not acute nutrient deprivation, and by demonstrating inhibition of lipophagy by Baf-A1 and chloroquine. Using this method, monensin was identified as a potent inducer of lipophagy, offering a new perspective for modulating lipid metabolism in diseases such as obesity and fatty liver disease. In summary, LD-Blue provides an effective tool to study dynamic formation of lipid droplets and lipophagy in metabolic lipid disorders and to evaluate lipophagy-targeted therapeutic agents.

Conflicts of interest

The authors declare no competing financial interest.

Data availability

Data are openly available to all readers.

Supplementary information (SI): synthesis and spectral analysis of new compounds, cytotoxicity and stability of the LD-Blue probe, time-course study, complete nutrient deficiency imaging, western blot analysis, analysis of inhibitor and so on. See DOI: https://doi.org/10.1039/d5an01241d.

Acknowledgements

This work was supported by grants to Dr S. Han from the Fundamental Research Funds for the Central Universities (20720240126) and NSF China (22177096). Dr J. Han was supported by NSF China (82388201), the National Key R&D Program of China (2020YFA0803500), the CAMS Innovation Fund for Medical Sciences (2019-I2M-5-062), the Fujian Province Central to Local Science and Technology Development Special Program (2022L3079) and the Fu-Xia-Quan Zi-Chuang District Cooperation Program (3502ZCQXT2022003). We thank Narong Yang for helpful discussions.

References

1 F. Wilfling, J. T. Haas, T. C. Walther and R. V. Farese, Lipid droplet biogenesis, *Curr. Opin. Cell Biol.*, 2014, **29**, 39–45.
2 E. Jarc and T. Petan, Lipid Droplets and the Management of Cellular Stress, *Yale J. Biol. Med.*, 2019, **92**(3), 435–452.
3 R. Singh, S. Kaushik, Y. Wang, Y. Xiang, I. Novak, M. Komatsu, K. Tanaka, A. M. Cuervo and M. J. Czaja, Autophagy regulates lipid metabolism, *Nature*, 2009, **458**(7242), 1131–1135.
4 D. W. Shin, Lipophagy: Molecular Mechanisms and Implications in Metabolic Disorders, *Mol. Cells*, 2020, **43**(8), 686–693.
5 (*a*) T. K. Fam, A. S. Klymchenko and M. Collot, Recent Advances in Fluorescent Probes for Lipid Droplets, *Materials*, 2018, **11**(9), 1–19; (*b*) Y. Zhao, W. Shi, X. Li and H. Ma, Recent advances in fluorescent probes for lipid droplets, *Chem. Commun.*, 2022, **58**(10), 1495–1509.
6 S. Bhuin, P. Chakraborty, P. Yogeeswari and M. Chakravarty, From Light to Insight: Harnessing Fluorescent Probes for Intracellular Pathway Visualization, *ACS Biomater. Sci. Eng.*, 2025, **11**(12), 6930–6996.
7 (*a*) A. H. Ashoka, P. Ashokkumar, Y. P. Kovtun and A. S. Klymchenko, Solvatochromic Near-Infrared Probe for Polarity Mapping of Biomembranes and Lipid Droplets in Cells under Stress, *J. Phys. Chem. Lett.*, 2019, **10**(10), 2414–2421; (*b*) X. Liu, X. Lu, T. Zhu, D. Wenli, Y. Zhenghui, H. Cao, S. Wang, Y. Tian, Z. Zhang, R. Zhang, S. C. De Souza and X. Tian, Revealing lipid droplets evolution at nanoscale under proteohormone stimulation by a BODIPY- hexylcarbazole derivative, *Biosens. Bioelectron.*, 2021, **175**, 112871.
8 (*a*) H. Xu, H. Zhang, G. Liu, L. Kong, X. Zhu, X. Tian, Z. Zhang, R. Zhang, Z. Wu, Y. Tian and H. Zhou, Coumarin-Based Fluorescent Probes for Super-resolution and Dynamic Tracking of Lipid Droplets, *Anal. Chem.*, 2019, **91**(1), 977–982; (*b*) G. Liu, J. Wang, G. Zhang, H. Zhang, Y. Zhu, H. Xu, L. Kong, Y. Tian, X. Zhu and H. Zhou, Dynamic cyclic behaviors of lipid droplets monitored by two-photon fluorescence probe with high photostability, *Spectrochim. Acta, Part A*, 2020, **228**, 117766; (*c*) T. Yoshihara, R. Maruyama, S. Shiozaki, K. Yamamoto, S.-I. Kato, Y. Nakamura and S. Tobita, Visualization of Lipid Droplets in Living Cells and Fatty Livers of Mice Based on the Fluorescence of π-Extended Coumarin Using Fluorescence Lifetime Imaging Microscopy, *Anal. Chem.*, 2020, **92**(7), 4996–5003; (*d*) F. Meng, J. Niu, H. Zhang, R. Yang, Q. Lu, G. Niu, Z. Liu and X. Yu, A pH-Sensitive Spirocyclization Strategy for Constructing a Single Fluorescent Probe Simultaneous Two-Color Visualizing of Lipid Droplets and Lysosomes and Monitoring of Lipophagy, *Anal. Chem.*, 2021, **93**(34), 11729–11735; (*e*) K.-N. Wang, L.-Y. Liu, D. Mao, S. Xu, C.-P. Tan, Q. Cao, Z.-W. Mao and B. Liu, A Polarity-Sensitive Ratiometric Fluorescence Probe for Monitoring Changes in Lipid Droplets and Nucleus during Ferroptosis, *Angew. Chem., Int. Ed.*, 2021, **60**(27), 15095–15100; (*f*) X. Li, C. Long, Y. Cui, F. Tao, X. Yu and W. Lin, Charge-Dependent Strategy Enables a Single Fluorescent Probe to Study the Interaction Relationship between Mitochondria and Lipid Droplets, *ACS Sens.*, 2021, **6**(4), 1595–1603; (*g*) M. Tian, E. Ge, B. Dong, Y. Zuo, Y. Zhao and W. Lin, Intramolecular Spirocyclization Enables Design of a Single Fluorescent

Probe for Monitoring the Interplay between Mitochondria and Lipid Droplets, *Anal. Chem.*, 2021, **93**(7), 3602–3610.

9 (*a*) P. Tan, W. Zhuang, S. Li, J. Zhang, H. Xu, L. Yang, Y. Liao, M. Chen and Q. Wei, A lipid droplet targeted fluorescent probe for high-efficiency image-guided photodynamic therapy of renal cell carcinoma, *Chem. Commun.*, 2021, **57**(8), 1046–1049; (*b*) S. Wang, X. Li, S. Y. Chong, X. Wang, H. Chen, C. Chen, L. G. Ng, J.-W. Wang and B. Liu, In Vivo Three-Photon Imaging of Lipids using Ultrabright Fluorogens with Aggregation-Induced Emission, *Adv. Mater.*, 2021, **33**(11), e2007490; (*c*) R. Zhang, G. Niu, Z. Liu, J. H. C. Chau, H. Su, M. M. S. Lee, Y. Gu, R. T. K. Kwok, J. W. Y. Lam and B. Z. Tang, Single AIEgen for multiple tasks: Imaging of dual organelles and evaluation of cell viability, *Biomaterials*, 2020, **242**, 119924.

10 (*a*) X. Zheng, W. Zhu, F. Ni, H. Ai, S. Gong, X. Zhou, J. L. Sessler and C. Yang, Simultaneous dual-colour tracking lipid droplets and lysosomes dynamics using a fluorescent probe, *Chem. Sci.*, 2019, **10**(8), 2342–2348; (*b*) J. Chen, C. Wang, W. Liu, Q. Qiao, H. Qi, W. Zhou, N. Xu, J. Li, H. Piao, D. Tan, X. Liu and Z. Xu, Stable Super-Resolution Imaging of Lipid Droplet Dynamics through a Buffer Strategy with a Hydrogen-Bond Sensitive Fluorogenic Probe, *Angew. Chem., Int. Ed.*, 2021, **60**(47), 25104–25113; (*c*) J. Chen, C. Wang, W. Liu, Q. Qiao, H. Qi, W. Zhou, N. Xu, J. Li, H. Piao, D. Tan, X. Liu and Z. Xu, Stable Super-Resolution Imaging of Lipid Droplet Dynamics through a Buffer Strategy with a Hydrogen-Bond Sensitive Fluorogenic Probe, *Angew. Chem., Int. Ed.*, 2021, **60**(47), 25104–25113; (*d*) Z.-L. Lai, J.-S. Chang, Y.-C. Chan, C.-C. Chang, C.-Y. Li and S.-W. Huang, Tumor tissues diagnosis with PIEE lipid droplet vesicles, *Sens. Actuators, B*, 2021, **330**, 129269.

11 S. Bhuin, P. Chakraborty, P. Yogeeswari and M. Chakravarty, Twisted Molecular Core Conjugated Oxo-Ether as a Fluorescent Probe for Lipid-Droplets Bioimaging and Live Cancer Cell Discrimination, *ACS Appl. Bio Mater.*, 2025, **8**(4), 2985–3001.

12 (*a*) S. Kaushik and A. M. Cuervo, Degradation of lipid droplet-associated proteins by chaperone-mediated autophagy facilitates lipolysis, *Nat. Cell Biol.*, 2015, **17**(6), 759–770; (*b*) M. Pu, W. Zheng, H. Zhang, W. Wan, C. Peng, X. Chen, X. Liu, Z. Xu, T. Zhou, Q. Sun, D. Neculai and W. Liu, ORP8 acts as a lipophagy receptor to mediate lipid droplet turnover, *Protein Cell*, 2023, **14**(9), 653–667.

13 (*a*) J. Zheng, S. Qin, L. Gui, H. Li, L. Fan, Y. Yang, H. Chen, H. Xu and Z. Yuan, Light-up lipid droplets for the visualization of lipophagy and atherosclerosis by coumarin-derived bioprobe, *Chin. Chem. Lett.*, 2021, **32**(8), 2385–2389; (*b*) W. Chen, N. Luo, Y. Zhang, L.-J. Tang, F. Wang and J.-H. Jiang, An activatable near-infrared fluorescent probe facilitated high-contrast lipophagic imaging in live cells, *Chem. Commun.*, 2021, **57**(69), 8664–8667; (*c*) M. Ghorpade, D. Rajput, P. Mahalingam and S. Kanvah, Live cell imaging of lipid droplets: fluorescent chalcones as probes for lipophagy and lipid–mitochondria interactions, *Mater. Chem. B*, 2025, **13**(4), 1338–1349; (*d*) R. Chen, Z. Li, C. Peng, L. Wen, L. Xiao and Y. Li, Rational Design of Novel Lipophilic Aggregation-Induced Emission Probes for Revealing the Dynamics of Lipid Droplets during Lipophagy and Ferroptosis, *Anal. Chem.*, 2022, **94**(39), 13432–13439; (*e*) W. Hu, L. Chai, X. Chen, J. Chen, H. Ren, C. Li, Y. Wang and T. D. James, Unveiling dynamic alterations of lipid droplet polarity during NAFLD-triggered lipophagy utilizing a far-red fluorescent probe with large stokes shift, *Sens. Actuators, B*, 2025, **422**, 1–8; (*f*) H. Wang, F. Tang, J. Yang, L. Hu, Y. Wang, X. Zhang, C. Zhang, X. Gu, C. Zhang and A. Ding, Washing-free fluorescent probes for visualizing the process of lipophagy and identifying non-alcoholic fatty liver disease, *Microchem. J.*, 2025, **208**, 1–9.

14 (*a*) A. Rohwedder, Q. Zhang, S. A. Rudge and M. J. O. Wakelam, Lipid droplet formation in response to oleic acid in Huh-7 cells is mediated by the fatty acid receptor FFAR4, *J. Cell Sci.*, 2014, **127**(Pt 14), 3104–3115; (*b*) Y. Fujimoto, H. Itabe, T. Kinoshita, K. J. Homma, J. Onoduka, M. Mori, S. Yamaguchi, M. Makita, Y. Higashi, A. Yamashita and T. Takano, Involvement of ACSL in local synthesis of neutral lipids in cytoplasmic lipid droplets in human hepatocyte HuH7, *J. Lipid Res.*, 2007, **48**(6), 1280–1292.

15 Y. Shi, X. Zou, S. Wen, L. Gao, J. Li, J. Han and S. Han, An organelle-directed chemical ligation approach enables dual-color detection of mitophagy, *Autophagy*, 2021, **17**(11), 3475–3490.

16 (*a*) T. M. Nthiga, B. K. Shrestha, J.-A. Bruun, K. B. Larsen, T. Lamark and T. Johansen, Regulation of Golgi turnover by CALCOCO1-mediated selective autophagy, *J. Cell Biol.*, 2021, **220**(6), 1–14; (*b*) L.-Q. Lu, M.-Z. Tang, Z.-H. Qi, S.-F. Huang, Y.-Q. He, D.-K. Li, L.-F. Li and L.-X. Chen, Regulation of the Golgi apparatus via GOLPH3-mediated new selective autophagy, *Life Sci.*, 2020, **253**, 117700; (*c*) K. L. Hickey, S. Swarup, I. R. Smith, J. C. Paoli, E. M. Whelan, J. A. Paulo and J. W. Harper, Proteome census upon nutrient stress reveals Golgiphagy membrane receptors, *Nature*, 2023, **623**(7985), 167–174.

17 A. Khaminets, T. Heinrich, M. Mari, P. Grumati, A. K. Huebner, M. Akutsu, L. Liebmann, A. Stolz, S. Nietzsche, N. Koch, M. Mauthe, I. Katona, B. Qualmann, J. Weis, F. Reggiori, I. Kurth, C. A. Hübner and I. Dikic, Regulation of endoplasmic reticulum turnover by selective autophagy, *Nature*, 2015, **522**(7556), 354–358.

18 A. S. Rambold, S. Cohen and J. Lippincott-Schwartz, Fatty acid trafficking in starved cells: regulation by lipid droplet lipolysis, autophagy, and mitochondrial fusion dynamics, *Dev. Cell*, 2015, **32**(6), 678–692.

19 T. Yoshimori, A. Yamamoto, Y. Moriyama, M. Futai and Y. Tashiro, Bafilomycin A1, a specific inhibitor of vacuolar-type H(+)-ATPase, inhibits acidification and protein degradation in lysosomes of cultured cells, *J. Cell Biol.*, 1991, **266**(26), 17707–17712.

20 M. Mauthe, I. Orhon, C. Rocchi, X. Zhou, M. Luhr, K.-J. Hijlkema, R. P. Coppes, N. Engedal, M. Mari and F. Reggiori, Chloroquine inhibits autophagic flux by decreasing autophagosome-lysosome fusion, *Autophagy*, 2018, **14**(8), 1435–1455.

21 S. Altshuler-Keylin, K. Shinoda, Y. Hasegawa, K. Ikeda, H. Hong, Q. Kang, Y. Yang, R. M. Perera, J. Debnath and S. Kajimura, Beige Adipocyte Maintenance Is Regulated by Autophagy-Induced Mitochondrial Clearance, *Cell Metab.*, 2016, **24**(3), 402–419.

22 J. R. Liang, E. Lingeman, T. Luong, S. Ahmed, M. Muhar, T. Nguyen, J. A. Olzmann and J. E. Corn, A Genome-wide ER-phagy Screen Highlights Key Roles of Mitochondrial Metabolism and ER-Resident UFMylation, *Cell*, 2020, **180**(6), 1160–1177.